SEARCH FOR $t\bar{t}Z' \to t\bar{t}t\bar{t}$ PRODUCTION IN THE MULTILEPTON FINAL STATE IN pp COLLISIONS AT $\sqrt{s} = 13$ AND 13.6 TEV WITH THE ATLAS DETECTOR

By

Hieu Le

A DISSERTATION

Submitted to
Michigan State University
in partial fulfillment of the requirements
for the degree of

Physics — Doctor of Philosophy

2025

ABSTRACT

Lorem ipsum dolor sit amet, consectetur adipiscing elit, sed do eiusmod tempor incididunt ut labore et dolore magna aliqua. Ut enim ad minim veniam, quis nostrud exercitation ullamco laboris nisi ut aliquip ex ea commodo consequat. Duis aute irure dolor in reprehenderit in voluptate velit esse cillum dolore eu fugiat nulla pariatur. Excepteur sint occaecat cupidatat non proident, sunt in culpa qui officia deserunt mollit anim id est laborum.

ACKNOWLEDGMENTS

Advisor: Reinhard Schwienhorst

Postdoc: Binbin Dong

Committee

MSU group

ATLAS analysis group

Friend: Daniel, Grayson, Bella, Eric, Jordan

Other friends: Jasper, Adam, Brittany

Parents

Spouse: Allen Sechrist

ATLAS in general & funding agencies

PREFACE

This is my preface. remarks remarks remarks

TABLE OF CONTENTS

List of Tables

List of Figures

KEY TO ABBREVIATIONS

Physical & mathematical quantities

χ^2 . . . . . chi-squared

ΔR . . . . . angular distance

η . . . . . pseudorapidity

E_{T} . . . . . transverse energy

$E_{\mathrm{T}}^{\mathrm{miss}}$/**MET** . missing transverse energy

$\hat{H}$ . . . . . Higgs oblique parameter

I . . . . . weak isospin

L . . . . . instantaneous luminosity

μ . . . . . signal strength

p_{T} . . . . . transverse momentum

Particles

b . . . . . bottom quark

pp . . . . . proton-proton

$t/\bar{t}$ . . . . . top/anti-top quark

$t\bar{t}t/t\bar{t}t\bar{t}$ . . . . three-/four-top-quark

tW . . . . . single-top

Acronyms

1LOS . . . . . one lepton, or two leptons of opposite charges

ATLAS . . . . A Toroidal LHC ApparatuS

BDT . . . . . boosted decision tree

BSM . . . . . Beyond the Standard Model

CERN . . . . European Organization for Nuclear Research

CMS . . . . . Compact Muon Solenoid

CR . . . . . control region

ECIDS . . . . Electron Charge ID Selector

GNN . . . . . graph neural network

HLT . . . . . High-Level Trigger

ID . . . . . inner detector

JER . . . . . jet energy resolution

JES . . . . . jet energy scale

JVT . . . . . Jet Vertex Tagger

L1 . . . . . Level 1

LH . . . . . likelihood

LLH . . . . . log-likelihood

LO . . . . . leading order

LAr . . . . . liquid argon

LHC . . . . . Large Hadron Collider

NF . . . . . normalization factor

NLO . . . . . next-to-leading order

NNLO . . . . next-to-next-to-leading order

NP . . . . . nuisance parameter

OP . . . . . operating point

PS . . . . . parton shower

PDF . . . . . parton distribution function

PCBT . . . . pseudo-continuous b-tagging

QED . . . . . quantum electrodynamics

QCD . . . . . quantum chromodynamics

QFT . . . . . quantum field theory

QmisID . . . charge mis-identification

SF . . . . . scale factor

SM . . . . . Standard Model

SR . . . . . signal region

SSML . . . . two leptons of the same charge, or more than two leptons (multilepton)

TDAQ . . . . Trigger and Data Acquisition

Roadmap

1. Finish adding bullets for all sections 04/04

   Remaining

   - introduction
   - higgs-top yukawa coupling, SMEFT & Higgs oblique parameter
   - collider physics
   - mc background samples
   - ttbar/ptrel/high pT calibration & results

2. Fill in details 04/18

   - Add missing figures
   - Add missing bib

3. Finalize analysis 04/30

4. String everything together

5. Miscellaneous/logistics (proofreading, review, ATLAS approval, etc.) 05/15

6. Submission to the graduate school 05/16

7. Defense 05/30

Chapter 1. Introduction

Chapter 2. Theoretical Overview

2.1 The Standard Model

- SM describes fundamental forces & elementary particles

- more descriptions (a bit of history + recent developments - higgs & neutrino masses) - limitations: gravity & general relativity, arbitrary free parameters

2.1.1 Elementary particles

- Bosons (Bose-Einstein statistics, integer spin) & fermions (Fermi-Dirac statistics, half-integer spin)

- Fermions - building blocks: quarks & leptons [protons/neutrons constituents?]

- Bosons - force carriers & interaction mediators (elementary bosons == gauge bosons

(chart of elementary particles here)

Fermions

- elementary particles

- half-integer spin

Quarks

- building blocks for hadrons & bosons

- up down —— charm strange —— bottom top [by order of discovery and mass]

- charge doublets: +2/3 and -1/3 charge

- color charge & color confinement in hadrons

- interacts with all 4 fundamental forces

Leptons

- electron —— muon —— tau + neutrino [by order of mass]

- charge -1, neutrinos charge neutral

- interacts with all forces except strong, neutrinos only weak and gravitational

Bosons

- force mediators

- integer spin

Scalar

- spin 0

- Higgs massive, charge neutral, provides rest mass for all elementary particles,

Vector

- spin 1

- W/Z (weak), photon (QED/electrodynamic), gluons (QCD/strong)

- photon/gluon massless, charge neutral, gluon carries color charge out of 8 combinations of quark colors (color octet)

- W/Z massive, charged/neutral

2.1.2 Mathematical formalism

- QFT: treats particles as excitations of corresponding quantum fields: fermion field ψ, electroweak boson fields $W_{1/2/3}$ & B, gluon field G_α, Higgs field ϕ

- Lagrangian: gauge QFT containing local gauge symmetries of $SU(3)_C \times SU(2)_L \times U(1)_Y$ and global Poincar symmetry: translational symmetry, rotational symmetry & special relativity frame invariance

- Noether's theorem: local symmetries -¿ strong/weak/EM, Poincar ¿ momentum, angular momentum & energy conservation

- unexpanded Lagrangian with description of each part: kinetic terms, coupling terms, mass/Higgs terms)

Quantum chromodynamics

- strong interaction, $SU(3)_C$ gauge group under Yang-Mills theory

- C = color charge conservation

- QCD Lagrangian, expansion & brief explanation

Electroweak

- unified weak & electromagnetic interactions, $SU(2)_L \times U(1)_Y$ gauge group

- L = left-handed chirality ¿ weak isospin (I) conservation

- Y = weak hyper charge conservation

- Q = charge conservation = $I_3 + 1/2Y$

- QED Lagrangian, expansion & brief explanation

Higgs mechanism

fermions & bosons still massless from previous section, resolved by introduction of the Higgs mechanism

(show Higgs field, potential & Lagrangian)

(show minimum of Higgs potential aka VEV)

————————————-[continue later]————————————-

2.1.3 Beyond the Standard Model

2.2 Four-top quark production

- Top: heaviest particle, strong coupling to many BSM particles in BSM models.

- 4top: xsec relevant to and enhanced by many BSM models

- Predicted by SM and observed [observation paper]

- Predicted xsec and observed xsec

- (insert Feynman diagrams)

- Decay products & final state topologies

Top-philic vector resonance

- (briefly introduce composite pseudo-nambu-Goldstone boson and motivation)

- hypothesis: top quark large mass results from high mixing between a "true" top quark and a colored, fermionic composite state

- composite vector resonance can be modeled as a top-philic Z' boson (without QCD color) or top-philic KK-gluon (with QCD color)

- color singlet vector boson (Z') model coupling strongly to top and weakly or not at all to others

- (show Lagrangian for interaction)

- two body decay Z' into $t\bar{t}$ with $m_{Z'}$ in TeV range $\rightarrow$ top mass

- decay channels: $t\bar{t}Z'$ s & t channels, tWZ', tjZ'

- (show decay width at LO)

- (Feynman diagrams here)

Higgs-top Yukawa coupling

(show Lagrangian of Higgs-top Yukawa coupling)

(show dependence of $t\bar{t}t\bar{t}$ xsec on Yukawa coupling at LO)

Effective field theory

SMEFT expanding on SM Lagrangian using higher order operators

(show EFT Lagrangian)

quick overview on SMEFT dimension-6 four-fermion operators for BSM interpretation

and Higgs oblique parameter

2.3 Collider physics

[pp collision, pdf, cross section, luminosity]

Luminosity

Proton-proton collisions

jets, parton shower, hadronization

Parton distribution function

Cross section

Chapter 3. LHC & ATLAS Experiment

3.1 The Large Hadron Collider

theoretical predictions are tested with experimental data obtained from particle accelerators

world's largest accelerator built by CERN situated on the border of Switzerland and France

has been operating since xxxx

lifetime divided into 3 runs, currently on Run 3 with planned upgrades on the horizon

responsible for a number of discoveries aka Higgs, etc.

3.1.1 Overview

[Basic info: location, size, main working mechanism, main detectors, main physics done]

- 27 km circumference, reusing LEP tunnels 175 m below ground level

- 7-13-13.6 TeV center of mass energies for pp collisions

- other than pp, also collides pPb, PbPb at 4 points with 4 main detectors: ATLAS, CMS (general purpose detectors), ALICE (heavy ion physics, ion collisions), LHCb (b-physics)

3.1.2 LHC operations

- focuses mainly on pp collisions for this thesis - beams split into bunches of 1.1×10^{11} protons with instantaneous luminosity of up to 2×10^{34} $\mathrm{cm}^{-2}\mathrm{s}^{-1}$

- beam energies ramp up in other accelerators before injection, full ramp up to 6.5 GeV about 20 minutes

(insert full diagram of accelerator chain)

Linac 4: hydrogen atoms, accelerated up to 160 MeV

PSB: H atoms stripped of electrons before injection, accelerated to 2 GeV

PS: 26 GeV, SPS: 450 GeV

LHC: injection in opposite directions, 6.5 TeV per beam

Run 1: 2010-2012, Run 2: 2015-2018, Run 3: 2022-2025, HL-LHC: 2029-?

COM energies: 7 & 8 TeV, 13 TeV, 13.6 TeV, 13.6 & 14 TeV

inbetween periods: long shutdowns (LS1, LS2, LS3)

(add HL-LHC timeline graph)

(insert LHC SM processes cross sections chart)

Top quark production at the LHC

history (CDF/D0)

LHC as a top factory: show luminosity and cross section for top processes

couples to Higgs as heaviest elementary particle

Higgs produced mainly from ggH (90%) via top loop and from ttH

(Feynman diagram of related processes)

3.2 The ATLAS detector

multipurpose particle detector with a symmetric cylindrical geometry and a solid angle coverage of almost 4π

44m long, 25m diameter

inner detector, solenoid/toroid magnet, EM & hadronic calorimeters, muon spectrometer

(insert figure)

right-handed cylindrical system, z-axis follows beamline, azimuthal and polar (0 in the beam direction) angles measured with respect to beam axis.

pseudorapidity $\eta = -\ln\tan(\theta/2)$, approaches $\pm$ inf along and 0 orthogonal to the beamline

distance $\Delta R = \sqrt{\Delta\eta^2 + \Delta\phi^2}$

transverse energy $E_{\mathrm{T}} = \sqrt{p_{\mathrm{T}}^2 + m^2}$

transverse momentum p_{T} component of momentum orthogonal to the beam axis $p_{\mathrm{T}} = \sqrt{p_x^2 + p_y^2}$

3.2.1 Inner detector

- measures tracks of charged particles with high momentum resolution ($\sigma_{p_{\mathrm{T}}}/p_{\mathrm{T}} = 0.05\% \pm 1\%$
- covers particles with $p_{\mathrm{T}} > 0.5$ GeV, $|\eta| < 2.5$

  pixel detector -¿ semiconductor tracker -¿ transition radiation tracker, innermost to outermost
- pixel detector:
  - innermost, 250 µm silicon pixel layers
  - detects charged particles from electron-hole pair production in silicon
  - measures impact parameter resolution & vertex identification for reconstruction of short-lived particles
  - spatial resolution of 10 µm in the $R - \phi$ plane and 115 µm in the z-direction
  - 80.4m readout channels
- sct:

- surrounds pixel detector, silicon microstrip layers with 80 µm strip pitch
- particle tracks cross 8 strip layers
- measures particle momentum, impact parameters, vertex position
- spatial resolution of 17 µm in the $R-\phi$ plane and 580 µm in the z-direction
- 6.3m readout channels.

- trt:
  - outermost, layers of 4 mm diameter gaseous straw tubes with transition radiation material (70% Xe + 27% CO_2 + 3% O_2) & 30 µm gold-plated wire in the center
  - tubes 144 cm length in barrel region ($|\eta| < 1$), 37 cm in the endcap region ($1 < |\eta| < 2$), arranged in wheels instead of parallel to beamline)
  - gas mixture produces transition radiation when ionized for electron identification
  - resolution/accuracty of 130 µm for each straw tube in the $R-\phi$ plane
  - 351k readout channels

3.2.2 Calorimeter systems

surrounds the inner detector & solenoid magnet, covers $|\eta| < 4.9$ and full ϕ range. Alternates passive and active material layers. Incoming particles passing through calorimeter produce EM cascades or hadronic showers in passive layer. Energies deposited and convert to electric signals in active layers for readout.

EM calorimeter:

- innermost, lead-LAr detector (passive-

active)

- measures EM cascades (bremsstrahlung & pair production) produced by electrons/photons
- divided into barrel region ($|\eta| < 1.475$) & endcap regions ($1.375 < |\eta| < 3.2$) with transition region ($1.372 < |\eta| < 1.52$) containing extra cooling materials for inner detector
- end-cap divided into outer wheel ($1.372 < |\eta| < 2.5$) & inner wheel ($2.5 < |\eta| < 3.2$)
- higher granularity in ID ($|\eta| < 2.5$) range for electrons/photons & precision physics, coarser elsewhere for jet reconstruction & MET measurements

hadronic calorimeter:

- outermost
- measures hadronic showers from inelastic QCD collisions
- thick enough to prevent most particles showers from reaching muon spectrometer
- split into tile calorimeter in barrel region ($|\eta| < 1.0$) & extended barrel region ($0.8 < |\eta| < 1.7$), LAr hadronic end-cap calorimeter (HEC) in end-cap regions ($1.5 < |\eta| < 3.2$) & LAr forward calorimeters (FCal) in $3.1 < |\eta| < 4.9$ range.
  - tile calorimeters: steel-plastic scintillating tiles, readout via photomultiplier tubes
  - hec: behind tile calorimeters, 2 wheels per end-cap. copper plates-LAr. overlap with other calorimeter systems to cover for gaps between subsystems
  - fcal: 1 copper module & 2 tungsten modules-LAr. copper optimized for EM measurements, tungsten for hadronic.

3.2.3 Muon spectrometer

- ATLAS outermost layer. measures muon momenta & charge in range $|\eta| < 2.7$
- momentum measured by deflection in track from toroid magnets producing magnetic field orthogonal to muon trajectory
  - large barrel toroids in $|\eta| < 1.4$, strength 0.5 T
  - 2 smaller end-cap toroids in $1.6 < |\eta| < 2.7$, strength 1 T
  - transition region $1.4 < |\eta| < 1.6$, deflection provided by a combination of barrel and end-cap magnets
- chambers installed in 3 cylindrical layers, around the beam axis in barrel region & in planes perpendicular to beam axis in the transition and end-cap regions
- split into high-precision tracking chambers (monitored drift tubes & cathode strip chambers) & trigger chambers (resistive plate chambers & thin gap chambers)
- trigger chambers provide fast muon multiplicity & approximate energy range information with L1 trigger logic
  - mdt:
    - range $|\eta| < 2.7$, innermost layer $|\eta| < 2.0$
    - precision momentum measurement
    - layers of 30 mm drift tubes filled with 93% Ar & 7% CO_2, with a 50 µm gold-plated tungsten-rhenium wire at the center
    - muons pass through tube, ionizing gas and providing signals. Combining signals from tubes

forms track

  * maximumn drift time from wall to wire 700 ns
  * resolution: 35 µm per chamber, 80 µm per tube

- csc:
  * forward region $2.0 < |\eta| < 2.7$, highest particle flux and density region
  * multiwire proportional chambers with higher granularity, filled with 80% Ar & 20% CO_2
  * shorter drift time than MDT, plus other features making CSC suitable for high particle densities and consequently able to handle background conditions
  * resolution: 40 µm in bending η-plane, 5 mm in nonbending ϕ-plane due to coarser cathode segmentation, per CSC plane

- rpc:
  * range $|\eta| < 1.05$
  * provide fast meas

- tgc:
  * range $1.05 < |\eta| < 2.7$

3.2.4 Forward detectors

- LUCID (LUminosity measurement using Cherenkov Integrating Detector): ±17 m from interaction point, measures luminosity using *pp* scattering in the forward region
- ALFA (Absolute Luminosity for ATLAS): ±240 m, measures *pp* scattering at small angles
- ZDC (Zero-Degree Calorimeter): ±140 m, measures centrality in heavy-ion collisions

3.2.5 Magnetic systems

superconducting solenoid & toroid magnets cooled to 4.5 K with liquid helium

solenoid: 2.56 m diameter, 5.8 m length, 2 T strength axial magnetic field, encloses inner detector

toroid = barrel + endcap toroid x2

barrel toroid: 9.2/20.1 m inner/outer diameter, 25.3 m length, 0.5 T strength

endcap toroid: 1.65/10.7 m inner/outer diameter, 5 m length, 1 T strength

(show magnet system diagram)

3.2.6 Trigger & data acquisition

LHC produces large amount of data (40 MHz with 25 ns bunch crossing), necessitates a way to filter out trash from interesting events

handles online processing, selecting and recording interesting events for further offline processing and more in-depth analyses

- Level-1 (L1) trigger: online, fast hardware-based trigger, reduces to 100 kHz
  - L1 calorimeter triggers (L1Calo): selects high energy objects & MET
  - L1 muon triggers (L1Muon): selects using hit information from RPC & TGC
  - L1 topological trigger (L1Topo): select based on topological selection synthesized using information from L1Calo & L1Muon
  - Central Trigger Processor (CTP): uses L1Calo/Muon/Topo for final L1 trigger decision within 2.5 μs latency. Also identify regions of interest in η and ϕ to be processed directly by HLT
- L1 trigger information read out by Front-End (FE) detector electronics then sent to ReadOut Drivers (ROD) for preprocessing and subsequently to ReadOut System (ROS) to buffer
- High-Level Trigger (HLT): offline, software-based trigger, using dedicated algorithms and L1 output as input, reduces to 1 kHz
- Send to storage for analyses after HLT

overall trigger process reduces original collision data rate by a factor of about 10000 after HLT

(show TDAQ diagram)

Chapter 4. Data & Simulated Samples

4.1 Data samples

LHC Run 2 data collected at $\sqrt{s} = 13$ TeV between 2015-2018

luminosity 140 fb^{-1}

(include uncertainty for Run 2 only)

4.2 Monte Carlo samples

4.2.1 $t\bar{t}Z'$ signal samples

Run 2 $t\bar{t}Z'$ sample

samples: 6 samples for each mass poin from $[1, 1.25, 1.5, 2, 2.5, 3]$ TeV

generator: MadGraph5_aMC@NLO v.2.8.1p3.atlas9 at LO with NNPDF3.1LO pdf

event: Pythia8 [v.244p3.rangefix] using A14 tune & NNPDF2.3LO pdf

parameters:

- chirality θ: does not affect the strong production mode for $t\bar{t}Z'$, therefore picking default value $\pi/4$ to suppress loop-production of the Z' resonance
- top coupling $c_t = 1$

resonance width computed with MadGraph5_aMC@NLO to be 4% of model configuration with these parameters

4.2.2 Background samples

Run 2 mc20 samples (2015-2018)

(show MC sample table)

(go in depth into each sample? briefly explain different generator, pdf and ps?)

Chapter 5. Particle Reconstruction & Identification

Reconstruction software reconstructs basic objects from signals collected from the event: interaction vertices, tracks, topological clusters of energy deposits

These quantities then used to reconstruct physics objects i.e. particles (electron, muon), jets, MET

5.1 Primary reconstruction

Topological clusters

[10][15]

Topological cluster (topo-cluster): Clusters of topologically connected cell signals in the calorimeter at the EM scale. This scale does not consider loss of signal from hadrons. Singular hits without hits from neighboring cells are considered noise.

Done in an effort to extract signal while minimizing electronic effects and physical fluctuations. Used to reconstruct hadronic objects and particles decaying hadronically i.e. τ leptons

Signal hits with significance above a cell signal significance level $\varsigma_{\text{cell}}^{\text{EM}}$ are seeded in as part of a proto-cluster. Neighboring cells satisfying a cluster growth threshold are collected into the cluster.

Two clusters are merged if a cell is matched to both

If a cluster has two or more local signal maxima satisfying $E_{\text{cell}}^{\text{EM}} > 500$ MeV, the cluster is split accordingly.

The process continues iteratively until all cells with significant signal efficiency have been matched to a cluster.

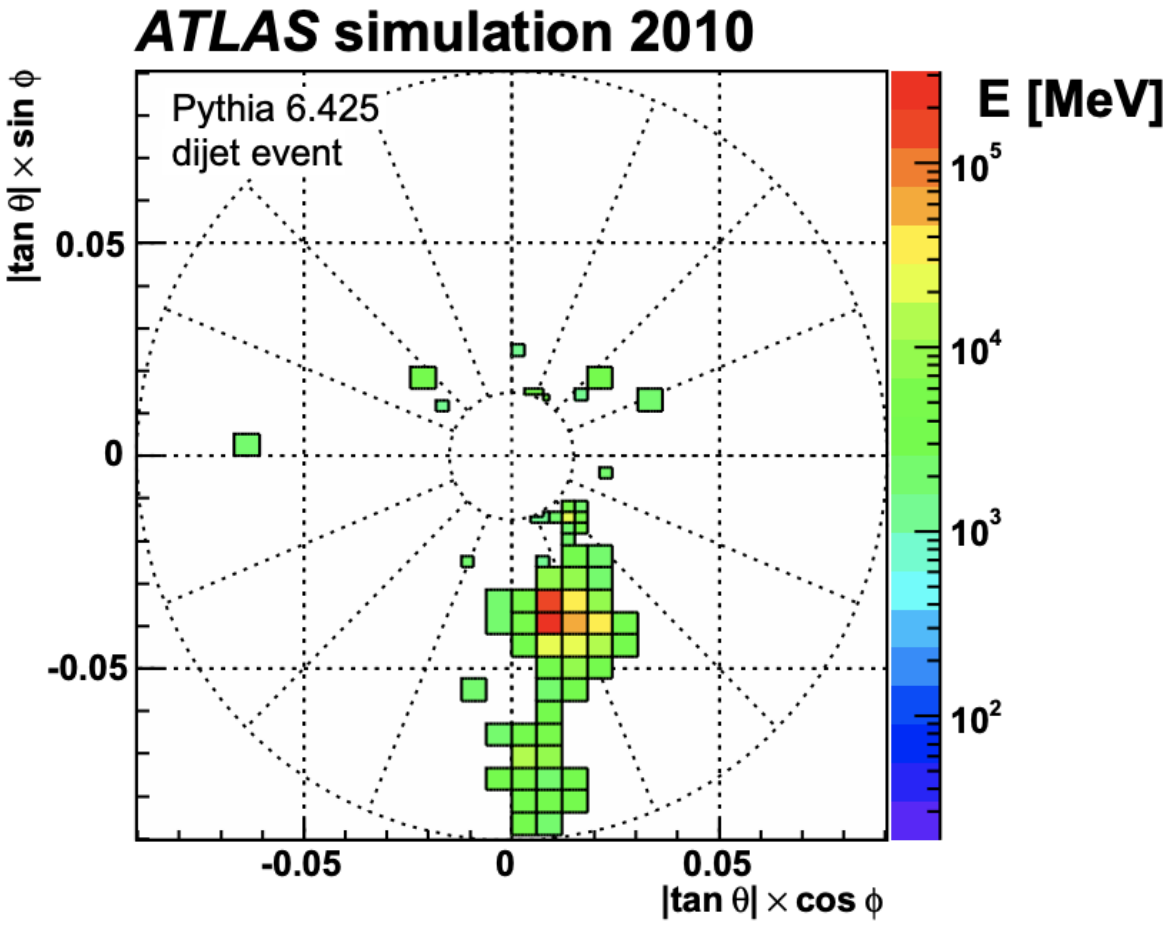

Figure 5.1

Tracks

[9]

Charged particles deposit energy in different layers of the inner detector and muon spectrometer

ID reco software: inside-out and outside-in algorithms

- Inside-out: [11]

  Starts with seeded hits in the silicon detector in pixel & SCT

  Loosely matched to an EM cluster to form a track candidate

  Hits are added to form a track candidate using a pattern recognition algorithm based on a Kalman filter formalism [14]

  Track candidates are then fitted with a χ^2 filter [12] and loosely matched to a fixed-sized EM cluster. Successfully matched track candidates are re-fitted with a Gaussian-sum filter (GSF) [6]

  This is followed by a track scoring strategy to resolve fake tracks & hit ambiguity between different tracks [19]

  Extend to TRT to form final tracks, filtered by threshold $p_{\mathrm{T}} > 400$ MeV.

- Outside-in: [16]

  Reverse, starts with segments in TRT extending inward to silicon hits in pixel & SCT

  Targeting secondary tracks (decays/interactions of primary particles) or long-lived particles

Vertices

Vertices: interaction or decay point

Primary vertex: pp interaction point

Important for reconstruction of the hard scattering pp interaction, resulting trajectories and

kinematic information of the event

- Vertex finding:

  Uses the z-position of a track as input

  Vertices require to have at least 2 tracks

  Iterative χ^2 algorithm evaluate track-vertex compatibility, using the track as new seed for another vertex if large discrepancy

- Vertex fitting:

  Adaptive multi-vertex fitter (AVF) algorithm assigns weights that depend on the track-vertex compatibility to each track to measure the probability of the track being an outlier vs inlier.

  Vertex is then estimated by iteratively minimizing an objective function of these weights

5.2 Jets

- Quarks, gluons & other non-color-neutral hadrons cannot be observed individually due to QCD color confinement

- A non-color-neutral hadron will almost immediately undergo hadronization producing a cone of color-neutral hadrons also known as a jet

- Jet signals can be used to reconstruct and consequently indirectly observe the original quarks/gluons the jets originated from

- Jet reconstruction:

- PFlow: energy deposited in the calorimeter systems by charged particles is removed and replaced by particle objects created with the remaining energy in the calorimeter and tracks matched to the topo-clusters. (include PFlow graphics)

- anti-k_t algorithms: sequential recombination jet algorithms

- pile-up jets: multiple interactions associated with one bunch crossing in addition to the hard scattering of interest and reconstructed as jets in the final states. Reconstructed pile-up jets can result from Pile-up jets are usually from soft interactions and can be distinguished with JVT algorithm using tracking information from the ID.

- JES/JER calibration: Jet reconstruction at EM scale does not accurately account for energy from QCD interactions and needs to be calibrated to jets reconstructed at particle level. This is done via a MC-based JES calibration sequence and additional JER calibration to match jet resolution in simulation to data using dijet events.

- reco setting: PFlow and anti-k_t algorithms with radius parameter $R = 0.4$, JVT applied to reconstructed jets with $p_{\mathrm{T}} < 60$ GeV and $|\eta| < 2.4$.

Flavor tagging

- Classification of hadronic jets is an important task for many LHC analyses especially ones studying final states (Higgs decay/4top)

- Flavor tagging is namely interested in identifying jets containing b-hadrons, c-hadrons, uds-hadrons (light-jets), and hadronic decays from τ.

- Of these, identifying b-jets is of particular interest due to their characteristically long lifetime (≈ 1.5 ps) from decay suppression by CKM factor, with a displaced secondary decay

vertex and usually a tertiary vertex from c-hadron decays.

Efficiency calibration

- [7]

- Performance of b-taggers are studied on MC simulated samples. However, the b-tagging efficiency predicted by simulation $\varepsilon_b^{\text{sim}}$ is usually not the same as the efficiency measured in data $\varepsilon_b^{\text{data}}$.

- The correction for the rate of events after applying a b-tagging requirement is calibrated and applied jet by jet in the form of data-to-simulation scale factors $\text{SF} = \varepsilon_b^{\text{data}}/\varepsilon_b^{\text{sim}}$.

- Usage of b-taggers are done via four operating points (OPs), corresponding to 60%, 70%, 77% and 85% b-jet tagging efficiency ε_b in simulated $t\bar{t}$ events in order from loosest to tightest discriminant cut points.

- OPs are defined by selection on the tagger output to provide a pre-defined level of ε_b, and act as a variable trade-off between the b-tagging true-positive rate (efficiency) and false-positive rate (purity)

- (insert TPR/FPR discriminant trade-off figure)

- ttbar calibration [1]

- ptrel and high pT calibration [18][8][2]

- impact parameter -> signed transverse impact parameter significance

- calibration results

GN2 b-tagging algorithm

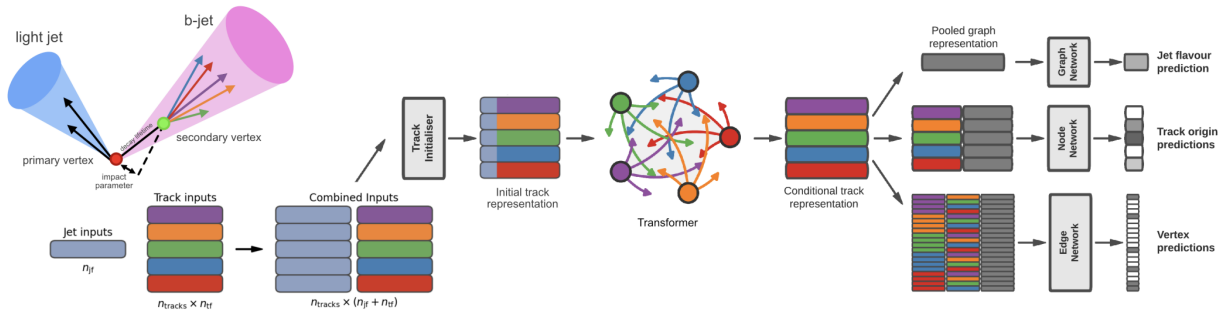

Figure 5.2: [5][13][17]

- GN2 transformer-based b-tagging algorithm, utilized for analysis of Run 2 and Run 3 data

- GN2 gives a factor of 1.5-4 improvement in experimental applications compared to the previous convolutional neural network-based standard b-tagging algorithm, DL1d, without dependence on the choice of MC event generator.

- Attention-based architecture, modified to incorporate domain knowledge and additional auxiliary physics objectives: grouping tracks originating from common vertices and prediction of the underlying process for each track

- MC simulated SM $t\bar{t}$ and BSM Z' events from pp collisions were used as training and evaluation samples. In order to minimize bias, both b- and light-jet samples are re-sampled to match c-jet distributions.

- GN2 concatenates 2 jet and 19 track reconstruction variables of up to 40 tracks to form the input feature vector, normalized to zero mean and unit variance.

- The output consists of a jet classification layer of size 4 consisting of p_b, p_c, p_u and p_τ for the probability of each jet being a b-, c-, light- or τ-jet respectively; a track-pairing output layer of size 2, and a track origin classification layer of 7 output categories.

5.3 Leptons

- Lepton reconstruction is concerned mainly with electron and muon construction, since tau decays quickly and can either be reconstructed using jets or light leptons. From here on out lepton will be used mostly to refer to electrons and muons

- Leptons can be classified into two categories: prompt leptons resulting from heavy particle decays, or non-prompt leptons resulting from detector or reconstruction effects, or from b- or c- hadron decays

- Reconstruction of leptons is therefore important to study the underlying physics and suppressing background

5.3.1 Electrons

- [4][3]

- Electrons lose energy interacting with the detector materials via bremsstrahlung. The bremsstrahlung photon can then produce an electron-positron pair which can itself leaves signals in the detector, creating a collimated object that can leave multiple tracks in the ID or EM showers in the calorimeter, all considered part of the same EM topo-cluster.

- Electron signal signature has three characteristic components: localized energy deposits in the calorimeter, multiple tracks in the ID and compatibility between the above tracks and energy clusters in the $\eta \times \phi$ plane. Electron reconstruction in ATLAS follows these steps accordingly - Seed-cluster reconstruction and track reconstruction are performed sequentially in accordance with the iterative clustering algorithm and track reconstruction method respectively, described in section 5.1

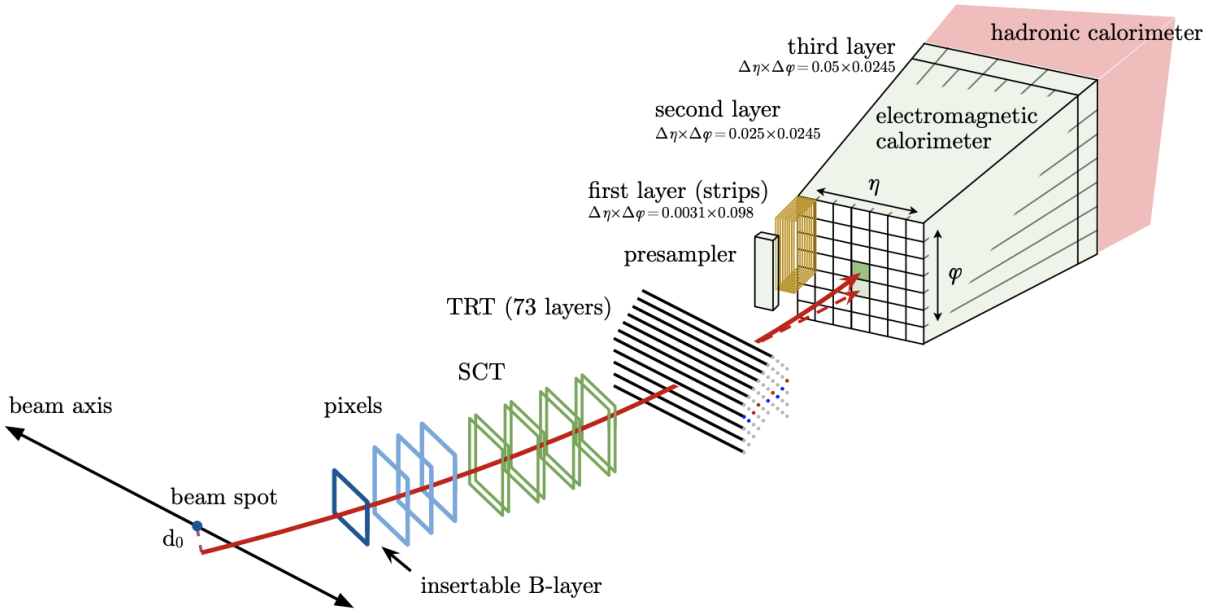

Figure 5.3

- The seed-cluster and track candidate not associated with a conversion vertex are then matched to form an electron candidate.

- A reconstructed cluster is expanded from the seed-cluster in either ϕ or η in the barrel or endcap region respectively

- The cluster energy is then calibrated to compute the original electron energy.

5.3.2 Muons

5.4 Missing transverse momentum

5.5 Pile-up & overlap removal

Chapter 6. Event Selection

[event selection criteria]

6.1 Object definition

[lepton pt cut study here]

6.2 Background estimation

6.2.1 Fake & non-prompt leptons

6.2.2 Irreducible background

6.3 Analysis regions

6.3.1 Control regions

$t\bar{t}W$ **CRs**

6.3.2 Signal regions

[include blinding strategy]

6.3.3 Validation region

6.4 Signal extraction

SM MVA

BSM MVA

Chapter 7. Systematic Uncertainties

7.1 Experimental uncertainties

7.2 Modeling uncertainties

7.2.1 Signal modeling uncertainties

7.2.2 Background modeling uncertainties

Chapter 8. Results

8.1 Likelihood fit

8.2 Limits

8.3 Interpretation

Chapter 9. Summary

References

[1] ATLAS Collaboration. *ATLAS b-jet identification performance and efficiency measurement with $t\bar{t}$ events in pp collisions at $\sqrt{s} = 13$ TeV*. In: *The European Physical Journal C* 79.11 (2019), p. 970. ISSN: 1434-6052. DOI: 10.1140/epjc/s10052-019-7450-8. arXiv: 1907.05120 [hep-ex] (cit. on p. 24).

[2] ATLAS Collaboration. *Dependence of the Jet Energy Scale on the Particle Content of Hadronic Jets in the ATLAS Detector Simulation*. ATL-PHYS-PUB-2022-021. 2022. URL: https://cds.cern.ch/record/2808016 (cit. on p. 24).

[3] ATLAS Collaboration. *Electron and photon performance measurements with the ATLAS detector using the 2015–2017 LHC proton–proton collision data*. In: *JINST* 14 (2019), P12006. DOI: 10.1088/1748-0221/14/12/P12006. arXiv: 1908.00005 [hep-ex] (cit. on p. 26).

[4] ATLAS Collaboration. *Electron reconstruction and identification efficiency measurements with the ATLAS detector using the 2011 LHC proton–proton collision data*. In: *Eur. Phys. J. C* 74 (2014), p. 2941. DOI: 10.1140/epjc/s10052-014-2941-0. arXiv: 1404.2240 [hep-ex] (cit. on p. 26).

[5] ATLAS Collaboration. *Graph Neural Network Jet Flavour Tagging with the ATLAS Detector*. ATL-PHYS-PUB-2022-027. 2022. URL: https://cds.cern.ch/record/2811135 (cit. on pp. viii, 25).

[6] ATLAS Collaboration. *Improved electron reconstruction in ATLAS using the Gaussian Sum Filter-based model for bremsstrahlung*. ATLAS-CONF-2012-047. 2012. URL: https://cds.cern.ch/record/1449796 (cit. on p. 21).

[7] ATLAS Collaboration. *Measurements of b-jet tagging efficiency with the ATLAS detector using $t\bar{t}$ events at $\sqrt{s} = 13$ TeV*. In: *JHEP* 08 (2018), p. 089. DOI: 10.1007/JHEP08(2018)089. arXiv: 1805.01845 [hep-ex] (cit. on p. 24).

[8] ATLAS Collaboration. *Measuring the b-jet identification efficiency for high p_T jets using multijet events in proton−proton collisions at $\sqrt{s} = 13$ TeV recorded with the ATLAS detector*. ATL-PHYS-PUB-2022-010. 2022. URL: https://cds.cern.ch/record/2804062 (cit. on p. 24).

[9] ATLAS Collaboration. *Performance of the ATLAS track reconstruction algorithms in dense environments in LHC Run 2*. In: *Eur. Phys. J. C* 77 (2017), p. 673. DOI: 10.1140/epjc/s10052-017-5225-7. arXiv: 1704.07983 [hep-ex] (cit. on p. 20).

[10] ATLAS Collaboration. *Topological cell clustering in the ATLAS calorimeters and its performance in LHC Run 1*. In: *Eur. Phys. J. C* 77 (2017), p. 490. DOI: 10.1140/epjc/s10052-017-5004-5. arXiv: 1603.02934 [hep-ex] (cit. on p. 19).

[11] T Cornelissen et al. *Concepts, Design and Implementation of the ATLAS New Tracking (NEWT)*. Tech. rep. Geneva: CERN, 2007. URL: https://cds.cern.ch/record/1020106 (cit. on p. 21).

[12] T G Cornelissen et al. *The global 2 track fitter in ATLAS*. In: *Journal of Physics: Conference Series* 119.3 (2008), p. 032013. DOI: 10.1088/1742-6596/119/3/032013. URL: https://dx.doi.org/10.1088/1742-6596/119/3/032013 (cit. on p. 21).

[13] Arnaud Duperrin. *Flavour tagging with graph neural networks with the ATLAS detector*. Tech. rep. Presented at DIS2023, Michigan State University, USA. Geneva: CERN, 2023. arXiv: 2306.04415 [hep-ex]. URL: https://cds.cern.ch/record/2860610 (cit. on pp. viii, 25).

[14] R. Frhwirth. *Application of Kalman filtering to track and vertex fitting*. In: *Nuclear Instruments and Methods in Physics Research Section A: Accelerators, Spectrometers, Detectors and Associated Equipment* 262.2 (1987), pp. 444–450. ISSN: 0168-9002. DOI: https://doi.org/10.1016/0168-9002(87)90887-4. URL: https://www.sciencedirect.com/science/article/pii/0168900287908874 (cit. on p. 21).

[15] Walter Lampl et al. *Calorimeter Clustering Algorithms: Description and Performance*. ATL-LARG-PUB-2008-002. 2008. URL: https://cds.cern.ch/record/1099735 (cit. on p. 19).

[16] Andreas Salzburger and on behalf of the ATLAS Collaboration. *Optimisation of the ATLAS Track Reconstruction Software for Run-2*. In: *Journal of Physics: Conference Series* 664.7 (2015), p. 072042. DOI: 10.1088/1742-6596/664/7/072042. URL: https://dx.doi.org/10.1088/1742-6596/664/7/072042 (cit. on p. 21).

[17] Samuel Van Stroud et al. *FTAG Run-3 Algorithms Performance*. Tech. rep. Geneva: CERN, 2023. URL: https://cds.cern.ch/record/2872884 (cit. on pp. viii, 25).

[18] Valentina Vecchio. *Measurement of the b-tagging efficiency using multi-jet events in ATLAS*. Tech. rep. Presented at The Tenth Annual Large Hadron Collider Physics

(LHCP2022). Geneva: CERN, 2022. URL: https://cds.cern.ch/record/2825428 (cit. on p. 24).

[19] D Wicke. *A New Algorithm for Solving Tracking Ambiguities*. In: (1998). URL: https://cds.cern.ch/record/2625731 (cit. on p. 21).